Pergamon

Continental Shelf Research, Vol. 14, No. 12, pp. 1293–1310, 1994
Elsevier Science Ltd
Printed in Great Britain.
0278-4343/94 $7.00 + 0.00

Mesoscale data assimilation studies in the Middle Adriatic Sea

SIMONA MASINA*† and NADIA PINARDI*

(*Received* 13 *February* 1992; *in revised form* 21 *July* 1993; *accepted* 26 *July* 1993)

Abstract—In this paper we describe a mesoscale data assimilation experiment in the Middle Adriatic Sea. In order to perform dynamical forecasts we provide a quasigeostrophic numerical model with a set of initial fields regularly gridded via an objective analysis technique. Maps of this initial condition show a surface intensified jet meandering around a cyclonic eddy at the thermocline and deep levels. We dynamically forecasted the flow evolution for 30 days after initialization. The time scale of the variability is of the order of a few weeks and the cyclonic vortex seems to be locked to the topography. A set of numerical experiments with different initial bottom boundary conditions, with and without topography, are made to explore the influence of the topographic constraint on the mesoscale flow evolution. As expected the influence of the topography on the dynamical evolution of the flow is very strong and it confines the jet–cyclone along the bathymetric contours, strengthening the flow. On the other hand the flow is not sensitive to changes in the density bottom initial condition.

Finally we analyze the energy and vorticity fields of the 1-month dynamical forecast experiment. It is concluded that a local frontogenetic process consisting of jet strengthening and cyclone development occurs and that available gravitational energy is converted into kinetic energy during the process.

1. INTRODUCTION

THE first mesoscale observations collected in the Middle Adriatic Sea (PASCHINI *et al.*, 1993) have confirmed the importance of the mesoscale signal in the Adriatic Sea and have shown its connections with the known general circulation flow (MALANOTTE-RIZZOLI and BERGAMASCO, 1983; ZORE-ARMANDA, 1956, 1963). Nevertheless, the mesoscale dynamics of this region are essentially unknown. In order to explain some aspects of the complex mesoscale variability it is necessary to conduct a coordinated program of modelling and experimental research because of the difficulty in sampling spatially with the required accuracy the physical fields of interest. This combination of data and models allows to study the dynamical balances of realistic mesoscale flow fields. The data assimilation approach has been tried with success in other regions of the world ocean especially by ROBINSON *et al.* (1986, 1987), PINARDI and ROBINSON (1987), WALSTAD and ROBINSON (1990) in the California Current System and in the western North Atlantic. In this first study in the Adriatic Sea, we will describe a set of mesoscale forecasts whose aim is to understand the main physical processes involved in the mesoscale eddy field of the Middle Adriatic Sea.

*Instituto per lo Studio delle Metodologie Geofisiche Ambientali, CNR, Modena, Italy.
†Present address: Program in Atmospheric and Oceanic Sciences, P.O. Box CN 710, Sayre Hall, Princeton, NJ 0845-0710, U.S.A.

The data of temperature and salinity were collected with mesoscale resolution during a cruise of 4 days in November 1988 (PASCHINI *et al.*, 1993). This data set allows us to calculate dynamic height and consequently the quasigeostrophic streamfunction at the model levels. Using statistical analysis and optimal interpolation techniques the streamfunction is then interpolated in a regularly gridded domain providing a set of maps, including the vorticity fields, used to initialize an open boundary baroclinic quasigeostrophic model. The model "predicts" the future evolution of the flow field for 30 days and we call this a dynamical forecast of the mesoscale flow field. The boundary conditions are persisted so that only the initial condition contains data information. Keeping the same initial and horizontal boundary conditions but changing the boundary conditions at the bottom we made a set of forecast experiments to show the typical time scales of the flow field. The next step, of course, will be the verification of the accuracy of the numerical forecasts.

In Section 2 we present the data set and the model design. Section 3 summarizes the numerical model used, the computational parameters and the bottom density boundary conditions. The objective mapping, regular gridding procedures and model initialization are presented in Section 4. Dynamical forecasts obtained by initializing and running the dynamical model forward in time are presented and analyzed in Section 5. The dynamical processes governing the local evolution of the fields in terms of a quasigeostrophic self-consistent energy and vorticity analysis scheme (EVA, PINARDI and ROBINSON, 1986) are explored in Section 6 and the conclusions are summarized in Section 7.

2. DATA SET AND MODEL DESIGN

The data set consists of a series of measurements collected during the period 7–11 November 1988, by the Italian research vessel *S. Lo Bianco* (PASCHINI *et al.*, 1993). The data consist of temperature and salinity profiles from 196 CTD casts. The stations cover an area of approximately 100×100 km^2 centered at 42.7°N and 15°E, rotated by 42° anticlockwise (see Fig. 1).

The sampling used in this cruise consists of highly resolved measurements made at a distance of 2 miles along eight transects separated from each other by a distance of 6 miles. This allows us to obtain a quasi-synoptic data set to resolve the mesoscale fields of the region.

The model used is the Harvard Open Ocean Model (ROBINSON and WALSTAD, 1987). It is a regional-dynamical model that has been developed for realistic local dynamical studies of fundamental processes and real data initialization. The model utilizes the quasigeostrophic (QG) equations which are appropriate for the mesoscale/synoptic variability in the ocean.

The horizontal resolution of the model is fixed to 2 km and the total domain is considered to be 42×46 gridpoints. The time step is 3 h. The data will be used as initial condition for the dynamical model.

The model has 12 levels in vertical which we chose to be located at 2.5, 10, 20, 30, 40, 50, 62.5, 77.5, 92.5, 107.5, 122.5 and 140 m.

At 150 m (the last model interface) we have defined the topography of the area which is shown in Fig. 2 for the model domain. It consists of a continental escarpment on its Northern, Southern western sides and a deep valley region, the Pomo and Jabuka Pits, in its center. The topographic depths are referred to 150 m (the mean depth of the basin) and

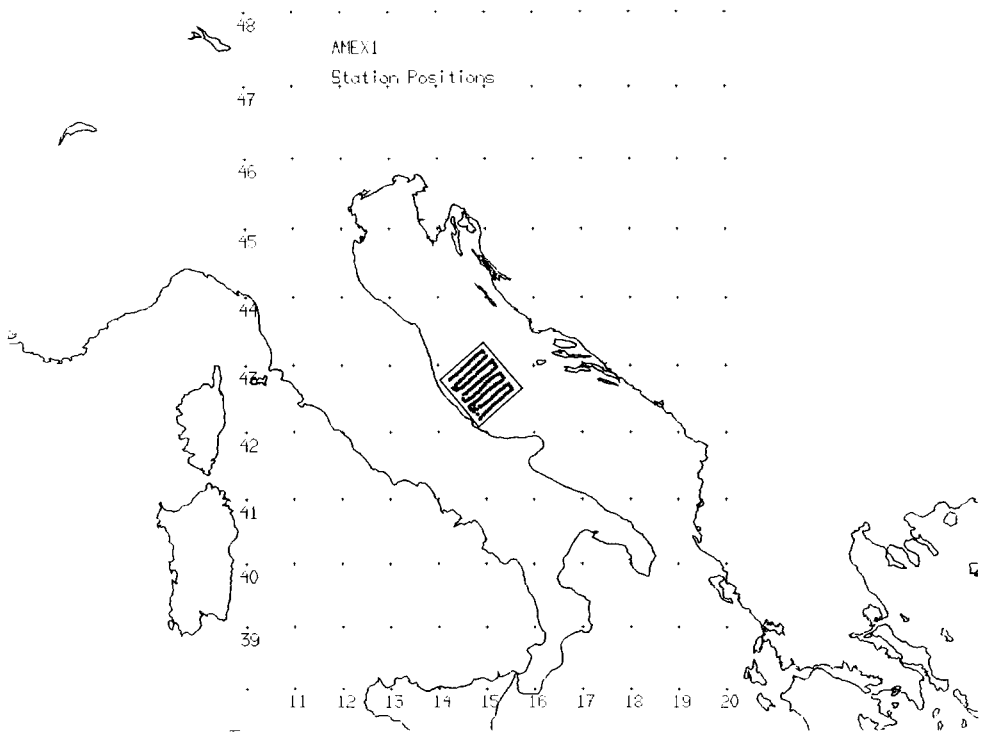

Fig. 1. The Mediterranean region with the CTD station locations.

we allow only for topographic excursions between 100 and 200 m. This produces in Fig. 2 a deeper continental shelf (about 80 m deeper) and a shallower region for the Pits (50 m shallower in a very small region) than in reality.

3. MODEL EQUATIONS AND PARAMETERS

The quasigeostrophic potential vorticity equation integrated by the model is written as

$$\frac{\partial q}{\partial t} + \alpha J(\psi,q) + \beta \frac{\partial \psi}{\partial x} = F \tag{1}$$

where

$$q = \nabla^2 \psi + \Gamma^2 \frac{\partial}{\partial z}\left(\sigma \frac{\partial \psi}{\partial z}\right) \tag{2}$$

and the Jacobian is defined as

$$J(\psi,q) = \frac{\partial \psi}{\partial x}\frac{\partial q}{\partial y} - \frac{\partial \psi}{\partial y}\frac{\partial q}{\partial x}.$$

The non-dimensional parameters are explained in Table 1.

The right hand side of equation (1), F, is the schematic representation of the Shapiro filter (SHAPIRO, 1970, 1971) applied to q. This filter removes small-scale vorticity which

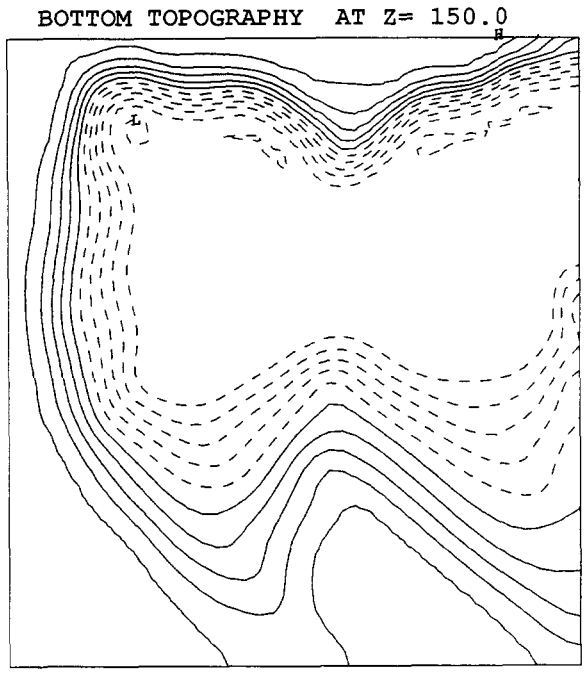

Fig. 2. Topography in model domain at 150 m.

Table 1. *List of symbols*

Symbol	Description
V_0	velocity scale = 1 cm s^{-1}
t_0	time scale = 5.8 days
L	horizontal scale = 5 km
f_0	Coriolis parameter at $\theta_0 = 43°$N (9.95×10^{-5} s^{-1})
β_0	$\partial f/\partial y\|_{\theta=\theta_0} = 1.67 \times 10^{-8}$ $(m\ s)^{-1}$
N_0^2	mid thermocline Brunt–Väisälä frequency value = 5.24×10^{-5} s^{-2}
H	vertical scale = 50 m
$N^2(z)$	climatological Brunt–Väisälä profile
α	$t_0 V_0/L = 1$
β	$\beta_0 t_0 L = 0.042$
Γ^2	$f_0^2 L^2/N_0^2 H^2 = 1.887$
σ	$N_0^2/N^2(z)$, stability profile
ψ	geostrophic streamfunction or pressure
q	dynamical vorticity
F	Shapiro filter

cascades from larger scales in non-linear flows via two-dimensional or geostrophic turbulence processes (RHINES, 1979) and that would eventually cause numerical instability. In this experiment we use a fourth-order Shapiro vorticity filter applied once every time step.

The computational model has been calibrated by HAIDVOGEL *et al.* (1980) and MILLER *et al.* (1983). It is finite element in the horizontal and the time evolution is calculated with an Adams–Bashford scheme. The model requires the specification of an initial condition ψ and for q and on the boundaries, at every time step, a boundary condition consisting of inflow and outflow streamfunction everywhere and vorticity on the inflow (CHARNEY *et al.*, 1950). In our study open boundary conditions are simplified, that is, they are persisted from the initial condition for the duration of the calculation.

Boundary conditions for the vertical part of (2) require the specification of $\partial\psi/\partial z$ at the top and bottom interfaces. These are referred to as top and bottom perturbation density fields since the vertical derivative of the geostrophic pressure field is the density anomaly with respect to the state of no motion density, assuming the hydrostatic relationship. It is important to point out that the model separates the variables for the $\psi(x, y, z, t)$ field by writing

$$\psi(x,y,z,t) = \sum_{j=1}^{N} \Phi_j(z)\Psi_j(x,y,t)$$

where $\Phi_j(z)$ are called the baroclinic modes and Ψ_j their respective horizontal amplitudes.

The flat bottom part of Φ_j, called Φ_j^f, is solution of

$$\Gamma^2 \frac{\partial}{\partial z}\left(\sigma(z)\frac{\partial \Phi_j^f}{\partial z}\right) = -\lambda_j^2 \Phi_j^f \tag{3}$$

with boundary conditions

$$\frac{\partial \Phi_j^f}{\partial z} = 0 \quad \text{at} \quad z = 0, -150\,\text{m}, \tag{4}$$

where Φ_j^f indicates the quasigeostrophic flat bottom baroclinic modes. The eigenvalues λ_j can be written as $\lambda_j^2 = L^2/R_j$, where L is the horizontal scale of the flow field (Table 1) and R_j the j^{th} internal Rossby radius of deformation. When the topography is considered the baroclinic modes will satisfy a value ψ_z given by the bottom density equation, that is

$$\sigma(z)\Gamma^2\left[\frac{\partial}{\partial t} + \alpha J(\psi,)\right]\frac{\partial \psi}{\partial z} = \vec{v}\cdot\nabla h \tag{5}$$

where $h(x, y)$ is the bottom relief (see ROBINSON and WALSTAD, 1987) and σ and Γ^2 are defined in Table 1. At the top interface we do not use wind stress curl and the modes satisfy (4) strictly.

To solve for equation (5) at the bottom interface we need initial density values and boundary condition values. A variety of bottom density initializations have been considered in general (MILLIFF, 1989). In our experiments we chose different bottom initial and boundary conditions as summarized in Table 2.

In order to solve (3) we first calculated the $N^2(z)$ profile from the average T, S profiles

using the Millero–Fofonoff algorithms (UNESCO, 1983). We considered only stations deeper than 100 m because we wanted to distinguish between coastally influenced and open ocean waters. The $N^2(z)$ profile is plotted in Fig 3(a). The results of the integration of (3) with 1 m vertical resolution are shown in Fig. 3(b) for the first three baroclinic modes. The first baroclinic mode has a zero crossing at 61 m and the second baroclinic mode has a maximum at about 60 m and the zero crossings at 33 and 108 m.

The choice of 12 levels appears to be able to reproduce very well the vertical structure of the dynamical modes as compared with the ones calculated with a grid size of 1 m. Fig. 3(c) shows the 12 levels first three dynamical modes. The first radius of deformation computed from the 1 m data is 3.64 km and from the 12 levels is 3.62 km. The second Rossby radius calculated with the 12 levels is 1.78 km instead of 1.77 km: the agreement is still very good.

4. THE STREAMFUNCTION FIELD: ANALYSIS PROCEDURE AND MODEL INITIALIZATION

To produce the streamfunction fields for model initialization and boundary conditions we calculated the dynamic height. This was computed at all the 12 model levels and the mean dynamic height profile was subtracted. The dynamic height anomaly, ΔD, between two pressure surfaces, p_1 and p_2, is written

$$\Delta D = \int_{p_1}^{p_2} \delta(p) dp$$

where

$$\delta = \frac{1}{\rho_{S,T}} - \frac{1}{\rho_{35,0}}$$

is the specific volume anomaly. The symbol Δ indicates the difference between the streamfunction at the level and the reference field at 140 m. Thus in our case the level of no motion is the lowest model level.

The dynamic height information, together with the assumption of geostrophy, gives us the streamfunction $\psi(x, y, z, t)$ defined as

$$\Delta\psi = \frac{\Delta D}{f_0}$$

where f_0 is the Coriolis parameter listed in Table 1.

To map ψ on the model grid we used a level-by-level objective analysis technique (BRETHERTON *et al.*, 1976; ROBINSON and LESLIE, 1985; CARTER and ROBINSON, 1986) assuming an homogeneous and isotropic correlation function of the form

$$C(r) = \left(1 - \frac{r^2}{a^2}\right) \exp\left(-\frac{r^2}{2b^2}\right); \qquad r^2 = x^2 + y^2$$

with the condition that $a \geq b\sqrt{2}$. The values chosen for a and b are 30 and 20 km respectively. Since $C(a) = 0$,a is called the zero-crossing length scale. The parameter b controls the exponential decay of the correlation function with distance, and it modulates large negative values of $C(r)$ outside the zero-crossing distance. The grid spacing for the interpolation is 2 km and the objective analysis is carried out using only 10 influential

points. The estimated normalized data error variance is 10%, considered to be representative of the environmental noise error for this measurement pattern.

From the interpolated streamfunction fields we compute the relative vorticity ($\nabla^2\psi$) and the thermal vorticity $\Gamma^2\,\partial/\partial z\,(\partial\psi/\partial z)$ fields. In Fig. 4 we show the initial streamfunction fields at each level of the model. The surface flow is dominated by a southward meandering jet while in the thermocline and deep levels a single eddy occupies the region with the same intensified jet at its border. The jet bifurcates around the southern border of the cyclonic eddy, one branch following its path south and the other turning eastward and intensifying the southern border of the cyclonic eddy.

5. DYNAMICAL FORECASTING

In this section we present the results of the forecast experiments made initializing the quasigeostrophic model with the analysis fields described in the previous section. The numerical experiments are summarized in Table 2.

In Fig. 5 we present the evolution of the C1 run (central experiment). In this case the bottom density initial condition was set equal to the density perturbation one interface above the bottom, e.g.

$$\left.\frac{\partial\psi}{\partial z}\right|_{bottom} = \left.\frac{\partial\psi}{\partial z}\right|_{(bottom-\Delta z)}$$

where the right hand side of the equation can be computed from the initial fields. The topography of Fig. 2 is used.

Five days after initialization, the cyclonic eddy is evident at 40 and 92.5 m in the central area of the domain. At the western side of the domain a positive structure is present at all the levels probably belonging to an anticyclonic eddy which we cannot resolve completely in our domain. At the deepest level we can notice a strong intensification of the jet formed between the western anticyclonic area and the cyclonic eddy. The flow field evolution for 30 days is dominated by the same structures with a clear intensification of both the jet and the cyclonic eddy at 92.5 and 122.5 m. Furthermore the cyclonic eddy undergoes a process of axisymmetrization at the end of the integration.

The maximum gradients in the jet are reached after 5 days at 122.5 m while between 5 and 30 days there is only a general readjustment of the field. This jet–cyclone strengthening event is called mesoscale frontogenesis and it was also observed by PINARDI and ROBINSON (1987) in the recirculation region of the Gulf Stream. There, a large anticyclonic pressure anomaly paired with a cyclonic eddy. This two eddies system developed a strong jet at their mutual border with the enhancement of both eddies. The phenomenology of the Adriatic case seems to be similar to the Atlantic.

In Fig. 6 we show the C2 experiment obtained without using topography and imposing the bottom initial and boundary condition $\partial\psi/\partial z = 0$. There are two clear differences between C2 and C1 runs. First of all in the C2 experiment the signal of the cyclone is totally misplaced or even lost at the deepest level (122.5 m). At this level the field is characterized by anticyclonic structures in the eastern part of the domain and by a cyclonic structure in the western part which has collapsed against the model boundary. At all the other levels the cyclone is much less intense and shifted westwards than in the central experiment. The comparison between C1 and C2 shows that the location of the eddy along the whole water

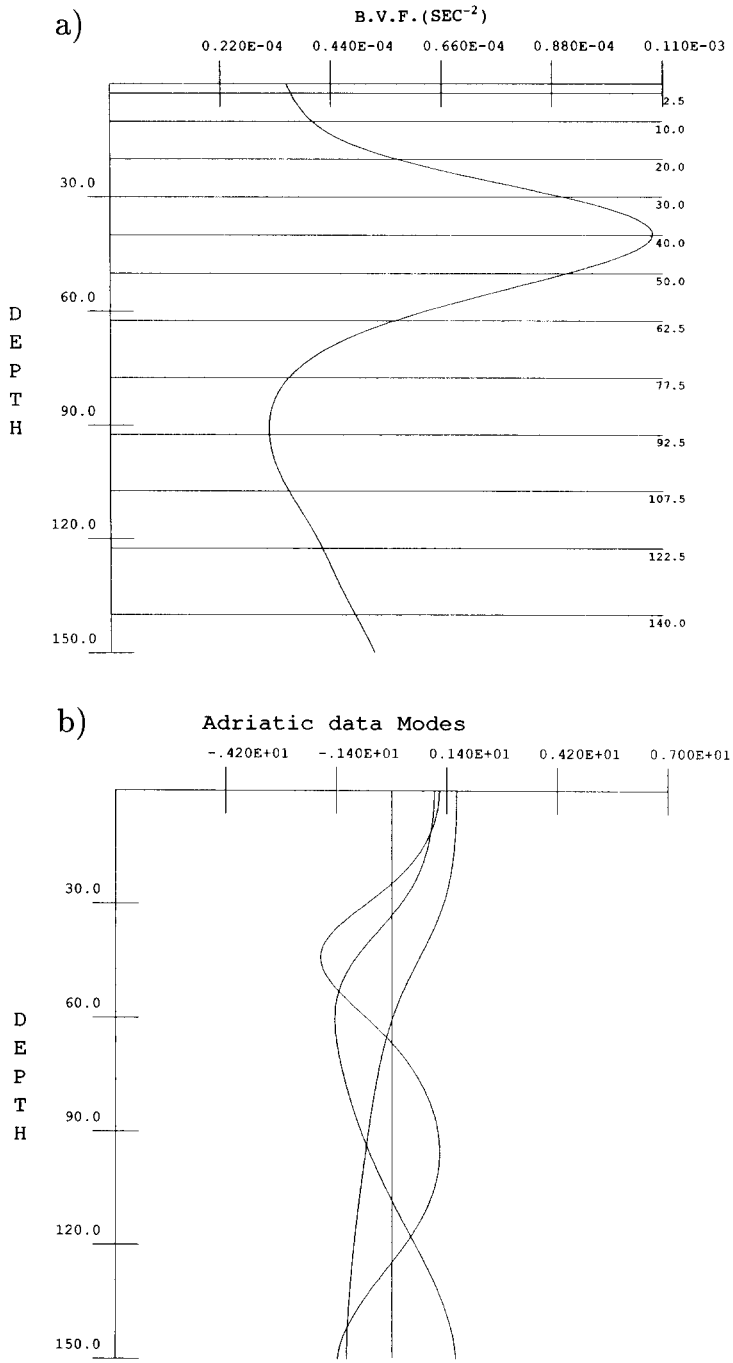

Fig. 3. (a) Brunt–Väisälä frequency vertical profile calculated from the T, S data set. The 12 vertical levels used in the model are superimposed. (b) First three baroclinic quasigeostrophic vertical modes calculated from the Brunt–Väisälä profile. (c) The first three eigenvectors calculated by the model.

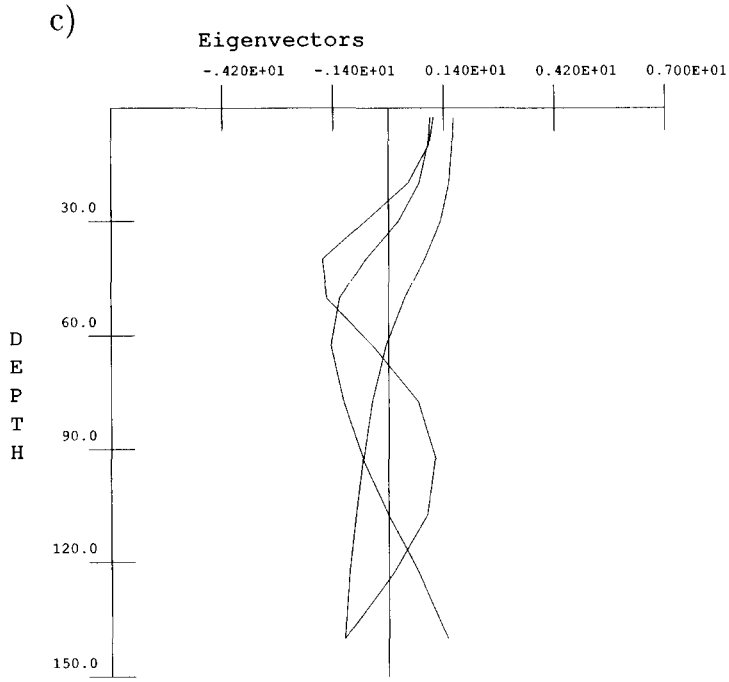

Fig. 3. *Continued.*

column and its strength during the 1 month integration is mostly due to the presence of the topography. Its absence causes the weakening and the displacement of the cyclone in the first five levels and its total misplacement at the last model level where the effect of the topography is of course much stronger.

In Fig. 7 we present the C3 experiment. It was obtained using the topography but imposing the initial and boundary bottom condition on $\partial\psi/\partial z$ equal to zero. The evolution of this run shows the presence of the cyclone in the same position and at the same levels as in the C1 run but weaker. The jet at the western border of the cyclonic eddy does not develop as strongly as in the C1 run.

In experiment C4 we tried another initial and boundary bottom $\partial\psi/\partial z$ condition. We can write the condition of "no-normal" flow over the bottom topography $h(x, y)$ as

$$w = -J[\psi,h(x,y)] \tag{6}$$

where the Jacobian has been defined before. Assuming no time dependence in (5) we can rewrite it using (6) as

$$J\left(\psi,h - \alpha\Gamma^2\sigma\frac{\partial\psi}{\partial z}\right) = 0. \tag{7}$$

Thus one solution of (7) is

$$\psi z|_{bottom} = \frac{h}{\sigma\alpha\Gamma^2}. \tag{8}$$

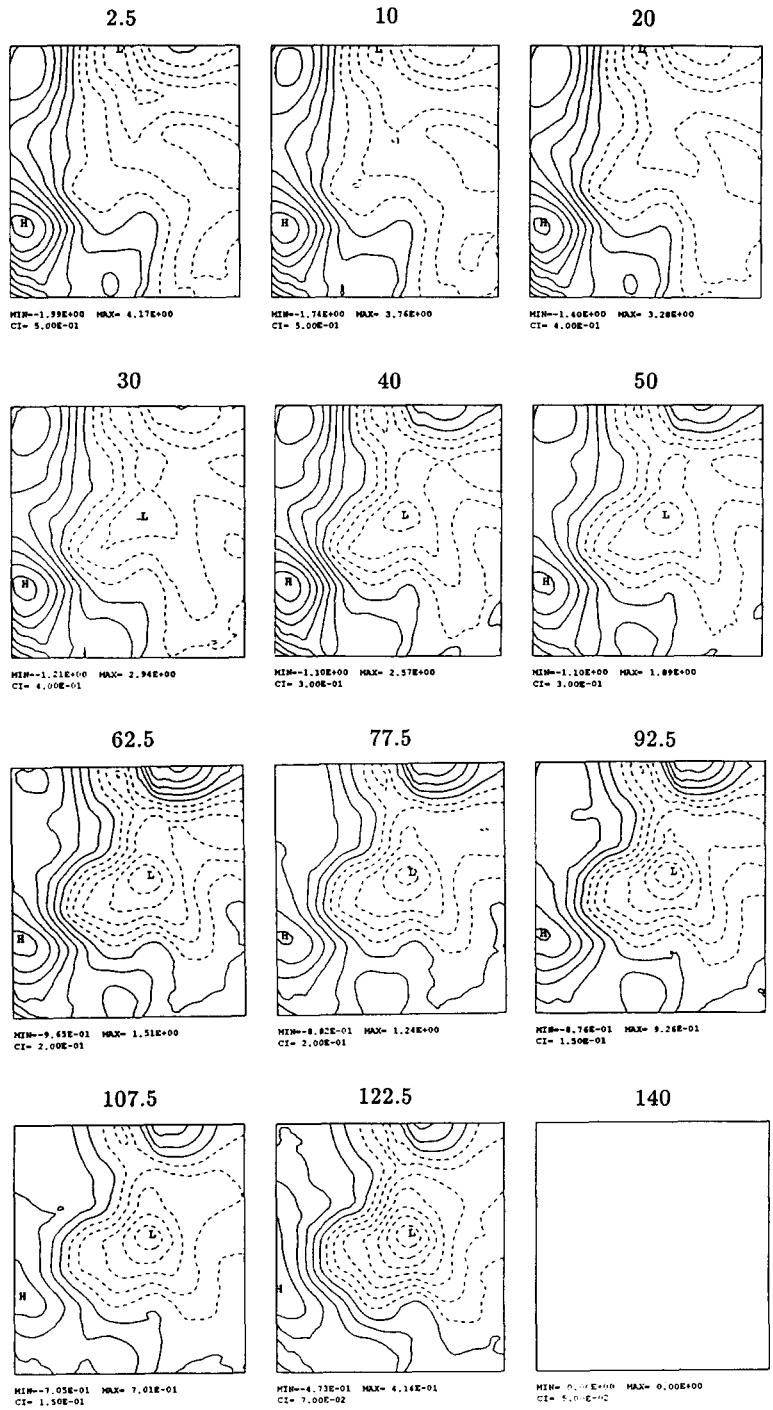

Fig. 4. Initial streamfunction fields at the 12 vertical levels (2.5, 10, 20, 30, 40, 50, 62.5, 77.5, 92.5, 107.5, 122.5 and 140 m).

Table 2. List of experiments

Run name	Run Descriptions
C1	topography and $\partial\psi/\partial z\|_{bottom} = \partial\psi/\partial z\|_{bottom-\Delta z}$, domain 42 × 46
C2	without topography and $\partial\psi/\partial z\|_{bottom} = 0$, domain 42 × 46
C3	topography and $\partial\psi/\partial z\|_{bottom} = 0$, domain 42 × 46
C4	topography and $\partial\psi/\partial z\|_{bottom} = h/\alpha\sigma\Gamma^2$ domain 42 × 46
C5	topography and $\partial\psi/\partial z\|_{bottom} = 0$, small domain 34 × 37

In Fig. 8 we show experiment C4 which uses the condition (8). The evolution of the streamfunction at all levels does not permit substantial differences with respect to the C1 run. Only at the deepest level the cyclone is not so axisymmetric as in C1 and it shows the presence of smaller-scale features.

We made also another experiment (C5, not shown) in a smaller domain that did not include the topographic step at the western boundary of the regular domain (the shelf break). The presence and the evolution of both the cyclone and the jet is not different from C1. This means that the stationarity of the cyclone is not due to the presence of the shelf break but it is prevalently locked by the topographic feature of the valley.

In conclusion the description and the interpretation of the dynamically forecasted fields indicate that the model results are very sensitive to the presence of topography while the use of different types of bottom density initial and boundary conditions is of secondary importance.

The evident persistence of the cyclone during the 30 days of free evolution of the flow field seems to suggest that the initialization fields were in an approximate geostrophic balance and that this period did not show any prominent propagation or change in the structure of the eddy field.

Even if the horizontal boundary conditions are kept constant and equal to their initial value the model produces reasonable fields, i.e. the fields were initially almost in geostrophic balance. The characteristic time scale of the jet–cyclone system seems to be at least of the order of several weeks.

6. ENERGY ANALYSIS OF FORECAST FIELDS

We present here the dynamical analysis of the process of frontogenesis occurring in the first 10 days of the model forecast. As explained by PINARDI and ROBINSON (1987), the jet and cyclone strengthening process is associated with a middle to low thermocline available gravitational to kinetic energy conversion, vertical export of energy from these levels to the upper thermocline levels and export of energy via horizontal pressure work divergences at all the levels.

As shown by PINARDI and ROBINSON (1986), a local growth of energy in the domain is associated with the growth of asymmetries in the energy conversion and redistribution terms of the kinetic and available gravitational energy equations. The kinetic energy (K) equation for a quasigeostrophic system is written

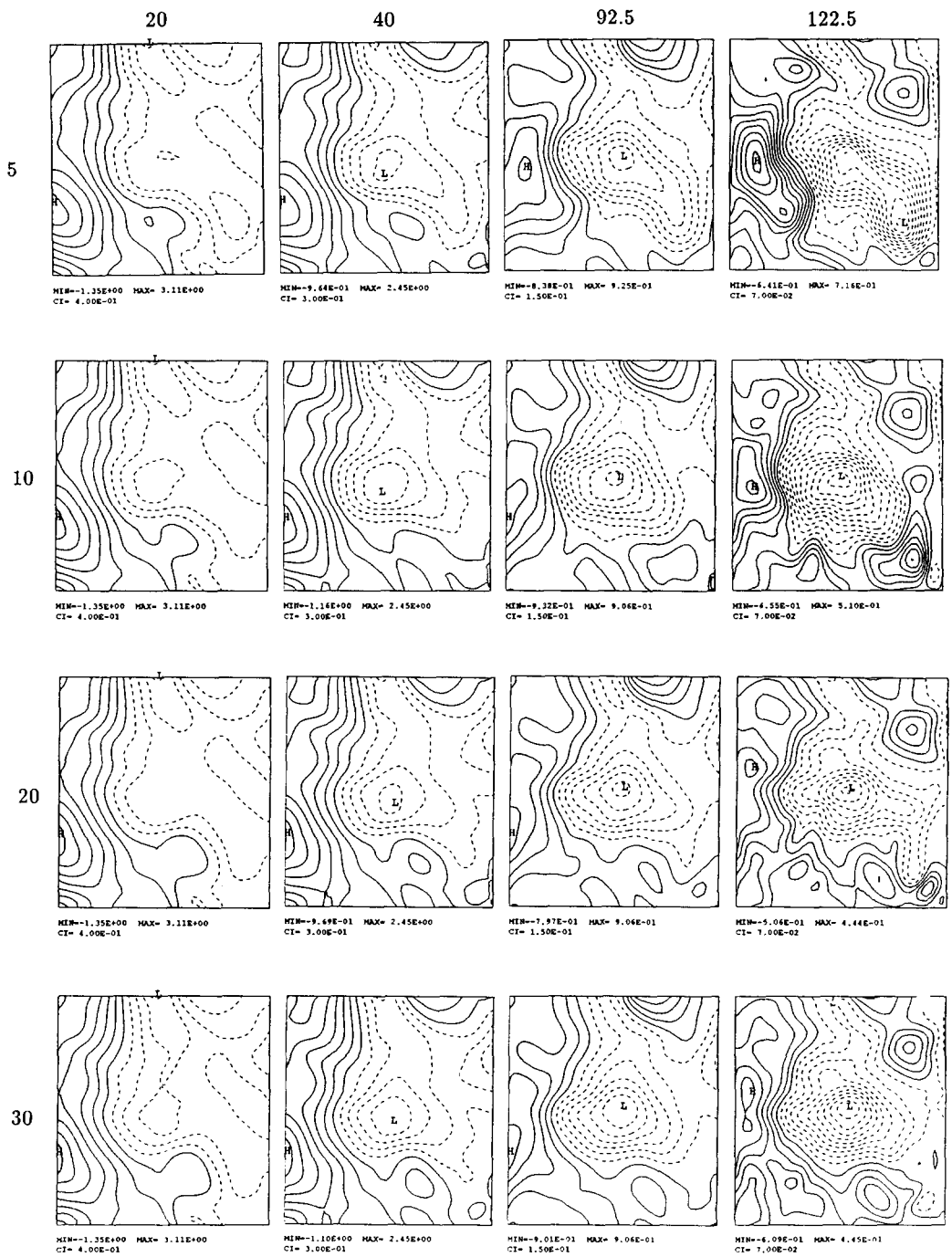

Fig. 5. C1 standard experiment streamfunction field. The levels plotted are written at the top of this picture. The time of integration is written on the left side and the maximum, minimum and contour interval used is displayed below each picture. Dashed contours correspond to negative values and continuous lines to positive values. The first dashed closed contour after a continuous line represents the zero contour level.

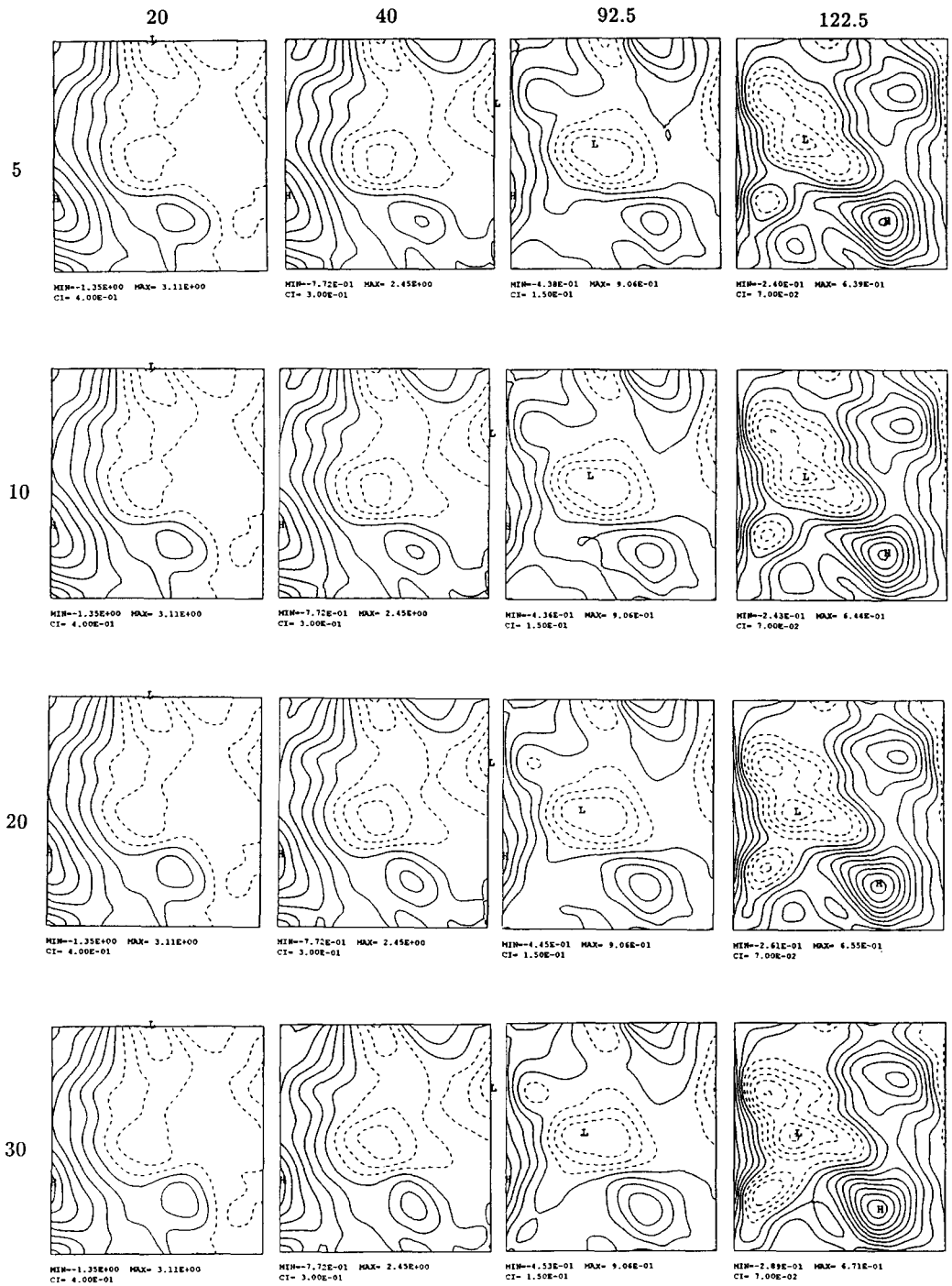

Fig. 6. As in Fig. 5 but for the C2 case.

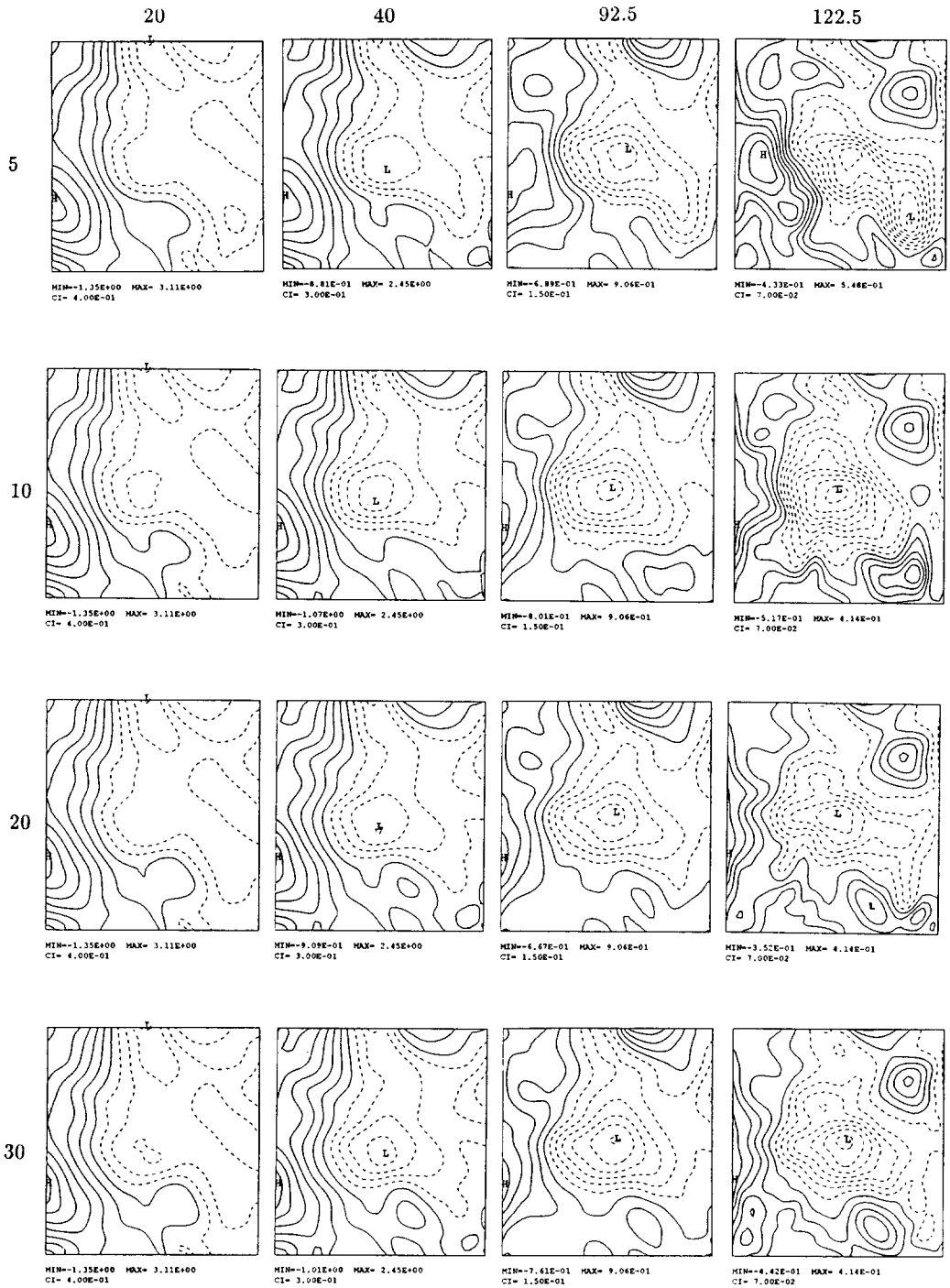

Fig. 7. As in Fig. 5 but for the C3 case.

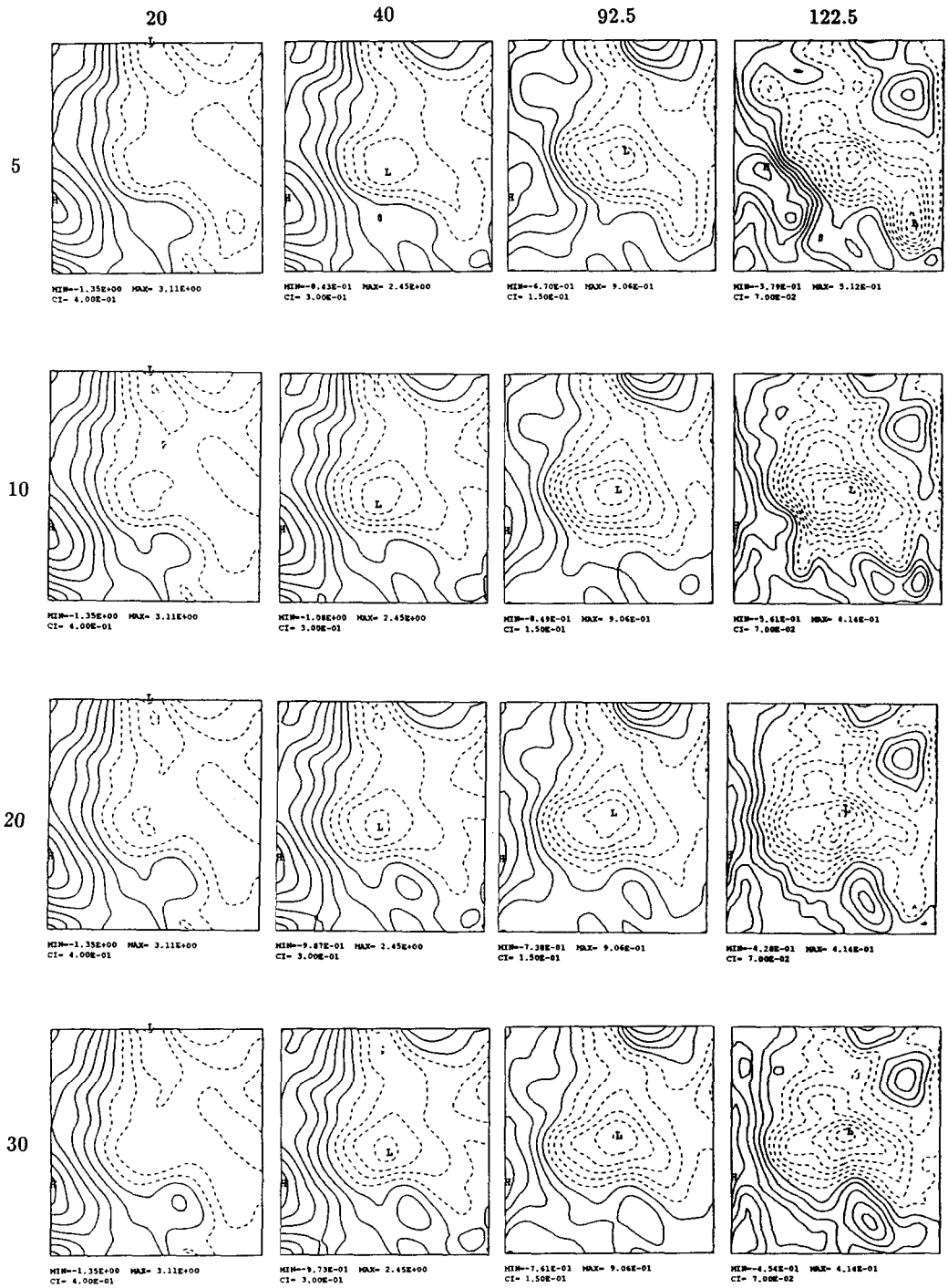

Fig. 8. As in Fig. 5 but for the C4 case.

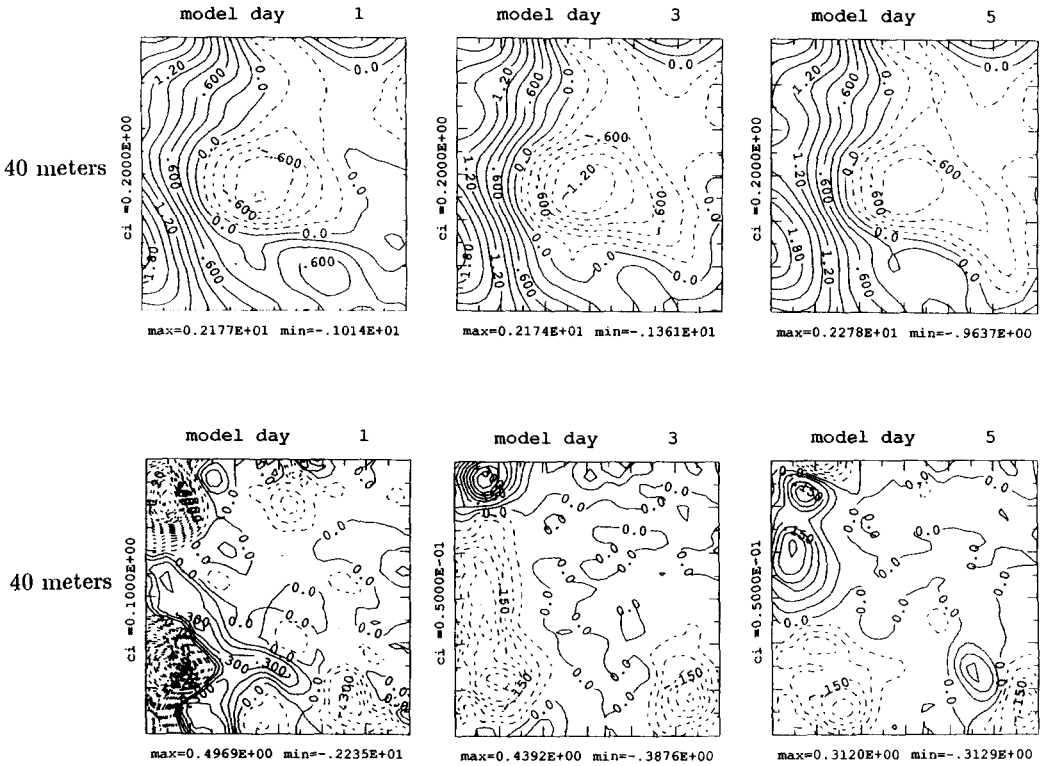

Fig. 9. Upper three figures: streamfunction fields at 40 m for days 1, 3 and 5 (indicated above the pictures) inside the forecast. Lower three figures: buoyancy work term maps at the same 3 days. The maximum, minimum of the field is indicated below the picture and the contour interval is written on the left side of each panel.

$$\frac{\partial}{\partial t} K = -\alpha \nabla \cdot (\vec{u} K) - \nabla \cdot (\psi \vec{u}) - \partial_z(\psi w) + \psi_z w + D \tag{9}$$

$$\dot{K} = \Delta F_k + \Delta F_\pi + \delta f_\pi + b + D \tag{10}$$

where the derivation of (9) is given in detail in PINARDI and ROBINSON (1986) and the symbols in (10) relate to their analytical expressions in (9). The equations (9) and (10) can be read in the following way: the local time rate of change of kinetic energy is equal to the sum of the horizontal divergence of advective kinetic energy flux (ΔF_k), the horizontal divergence of pressure work (ΔF_π), the vertical divergence of pressure work (δf_π), the buoyancy work (b) and the symbolic representation of the dissipation term due to the Shapiro filter on the vorticity (D).

In Fig. 9 we present the streamfunction and the buoyancy work term defined as "b" in equation (10). The fields are shown at 40 m where the maximum conversion occurs. The conversion term shows the growth of a negative pole along the jet at the border of the cyclone, which already decays in amplitude at day 5. The sign of this "burst" of baroclinic conversion is such that available gravitational energy is converted to kinetic energy, as expected in a process of baroclinic amplification of a frontal structure.

The area average in the domain of Fig. 9 of each term in (9) is given in Fig. 10. The

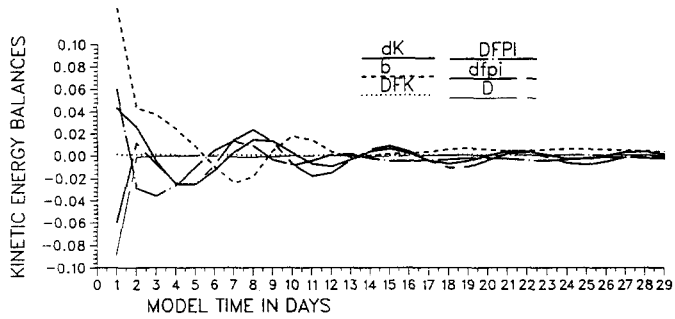

Fig. 10. Integrated kinetic energy terms [see equation (6)] vs time. The different curves meaning is indicated on the upper right corner of the figure.

kinetic energy converted from the available gravitational energy is locally redistributed by δf_π and ΔF_π terms which export energy from the region of the jet–cyclone structure vertically and horizontally. In conclusion, the mesoscale eddy field of the Middle Adriatic Sea shows processes typical of open ocean mesoscale fields, like frontogenesis and cyclone development. Thus the Middle Adriatic mesoscale currents might have a dynamical behaviour typical of open ocean regions.

7. CONCLUSIONS

In this paper we have presented the initialization of a regional quasigeostrophic model in the Middle Adriatic Sea. The mesoscale eddy field has been previously mapped by PASCHINI *et al.* (1993) using the first mesoscale data set collected in the region. The field consisted of a cyclone located on the southward side of a topographic valley formed by the Pomo and Jabuka Pits in the Middle Adriatic Sea. The data were used to obtain the initial and boundary conditions for a quasigeostrophic regional model which has been integrated in a forecast mode for 30 days. This model has been shown previously (PINARDI and ROBINSON, 1987; WALSTAD and ROBINSON, 1990) to give accurate forecasts of the mesoscale eddy fields of other world ocean basins.

The dynamical evolution of the flow field consists of a cyclone adjustment process which produces a local frontogenesis process at one of its borders, deepening of the cyclone signature and slow westward motion of the cyclonic center.

The topography is shown to be extremely important for the maintenance and correct positioning of the cyclonic eddy at the center of the domain. Its absence produces a smaller and weaker cyclone and a very strong jet along the western side of the model domain. This dynamical behaviour seems to be more unrealistic than the case with topography.

The local frontogenesis and cyclone development processes occurring during the forecast experiment are characteristic of open ocean eddy fields, suggesting that the dynamics in the deep part of the Middle Adriatic Sea might be similar to the other world open ocean eddy fields.

An interesting aspect of the future research in the Adriatic could be the study of the influence of this eddy field on the coastal circulation. The slow eddy field motion indicated by the forecast experiment could indicate that, once the eddy field has established itself, not much interaction is occurring between the shelf and deep areas of the Middle Adriatic.

We hope that showing the feasibility of an open ocean mesoscale forecast in the region would help to plan adequate surveys to explore coastal and deep ocean interactions.

Acknowledgements—This work has been supported by the Progetto Strategico Adriatico of the Italian C. N. R. Simona Masina was supported by a grant given to I. M. G. A. by the Progetto Finalizzato "Calcolo Parallelo".

REFERENCES

BRETHERTON F. P., R. E. DAVIS and C. B. FANDRY (1976) A technique for objective analysis and design of oceanographic experiments. *Deep-Sea Research*, **23**, 559–582.

CARTER E. F. and A. R. ROBINSON (1987) Analysis models for the estimation of oceanic fields. *Journal of Atmospheric and Oceanic Technology*, **4**(1), 49–74.

CHARNEY J. G., R. FJORTOFT and J. VON NEUMANN (1950) Numerical integration of the barotropic vorticity equation. *Tellus*, **2**, 237.

HAIDVOGEL D. B., A. R. ROBINSON and E. E. SCHULMANN (1980) The accuracy, efficiency and stability of three numerical models with application to open ocean problems. *Journal of Computational Physics*, **34**, 1–53.

MALANOTTE-RIZZOLI P. and A. BERGAMASCO (1983) The dynamics of the coastal region of the Adriatic Sea. *Journal of Physical Oceanography*, **13**, 1105–1130.

MILLER R. N., A. R. ROBINSON and D. B. HAIDVOGEL (1983) A baroclinic quasigeostrophic open ocean model. *Journal of Computational Physics*, **50**, 38–70.

MILLIFF A. R. (1989) Quasigeostrophic ocean flows in coastal domains, Ph.D. Thesis, Harvard University.

PASCHINI E., A. ARTEGIANI and N. PINARDI (1993) The mesoscale eddy field of the Middle Adriatic Sea. *Deep-Sea Research*, **40**, 1365–1377.

PINARDI N. and A. R. ROBINSON (1986) Quasigeostrophic energetics of open ocean regions. *Dynamics of Atmospheres and Oceans*, **10**, 185–219.

PINARDI N. and A. R. ROBINSON (1987) Dynamics of deep thermocline jets in the POLYMODE Region. *Journal of Physical Oceanography*, **17**, 1163–1188.

RHINES P. B. (1979) Geostrophic turbulence. *Annual Review of Fluid Mechanics*, **11**, 401–441.

ROBINSON A. R. and W. G. LESLIE (1985) Estimation and prediction of oceanic eddy fields. *Progress in Oceanography*, **14**, 485–510.

ROBINSON A. R., J. A. CARTON, N. PINARDI and C. N. K. MOOERS (1986) Dynamical forecasting and dynamical interpolation: an experiment in the California Current. *Journal of Physical Oceanography*, **16**, 1561–1579.

ROBINSON A. R. and L. J. WALSTAD (1987) The Harvard Open Ocean Model: calibration and application to dynamical process, forecasting and data assimilation studies. *Journal of Applied Numerical Mathematics*, **3**, 89–131.

SHAPIRO R. (1970) Smoothing, filtering and boundary effects. *Review of Geophysics and Space Physics*, **2**, 491–507.

SHAPIRO R. (1971) The use of linear filtering as a parameterization for atmospheric diffusion. *Journal of Atmospheric Science*, **28** 523–531.

UNESCO (1983) *Algorithms for computation of fundamental properties of seawater*. N. P. FOFONOFF and R. C. MILLARD Jr, editors, Technical papers in marine science, **44**.

WALSTAD L. J. and A. R. ROBINSON (1990) Hindcasting and forecasting of the POLYMODE data set with the Harvard Open-Ocean Model. *Journal of Physical Oceanography*, **20**, 1682–1702.

ZORE-ARMANDA M. (1956) On gradient currents in the Adriatic Sea. *Acta Adriatica*, **8**, 1–38.

ZORE-ARMANDA M. (1963) Les masses d'eaux de la Mer Adriatique. *Acta Adriatica*, **10**, 1–94.